Chemical and Structural Variety in Sodium Thioarsenate Glasses Studied by Neutron Diffraction and Supported by First-Principles Simulations

Mohammad Kassem, Tinehinane Bounazef, Daniele Fontanari, Anton Sokolov, Maria Bokova, Alex C Hannon, Eugene Bychkov

Chemical and Structural Variety in Sodium Thioarsenate Glasses Studied by Neutron Diffraction and Supported by First-Principles Simulations

Mohammad Kassem,[1] Tinehinane Bounazef,[1] Daniele Fontanari,[1] Anton Sokolov,[1] Maria Bokova,[1] Alex C. Hannon,[2] and Eugene Bychkov*,[1]

[1] Laboratoire de Physico-Chimie de l'Atmosphère, Université du Littoral Côte d'Opale, 59140 Dunkerque, France

[2] ISIS Facility, Rutherford Appleton Laboratory, Chilton, Didcot, OX11 0QX, U.K.

ABSTRACT: Sodium conducting sulfide glasses are promising materials for new generation of solid-state batteries. Deep insight into the glass structure is required to ensure a functional design and tailoring of vitreous alloys for energy applications. Using pulsed neutron diffraction supported by first-principles molecular dynamics, we show a structural diversity of Na_2S-As_2S_3 sodium thioarsenate glasses, consisting of long corner-sharing (CS) pyramidal chains CS-$(AsSS_{2/2})_k$, small As_pS_q rings, $p+q \leq 11$, mixed corner- and edge-sharing oligomers, edge-sharing (ES) dimers ES-As_2S_4, isolated (ISO) pyramids ISO-AsS_3, entirely or partially connected by sodium species. Polysulfide S-S bridges and structural units with homopolar As-As bonds complete the glass structure, basically different from structural motifs predicted by the equilibrium phase diagram. In contrast to superionic silver and sodium sulfide glasses, characterized by a significant population of isolated sulfur species S_{iso}, $0.20 < S_{iso}/S_{tot} < 0.28$, that is, sulfur connected only to mobile cations M^+ with a usual stoichiometry $M/S_{iso} = 2$, poorly conducting Na_2S-As_2S_3 alloys exhibit a modest S_{iso} fraction of 6.2 %.

1. INTRODUCTION

Crystalline and glassy Na^+ conducting sulfide electrolytes appear to be promising materials for all-solid-state rechargeable batteries in large-scale stationary energy storage applications.[1-5] Recent interest in superionic sodium conductors was focused on specific crystal structures consisting of 3D tunnels for fast ion migration over an open space around lattice-forming polyhedra, that is, PS_4 or SbS_4 tetrahedra with additional cationic vacancies.[6-8] On the other hand, functional properties of sodium sulfide vitreous alloys are strongly dependent on the short and intermediate range order in the glass network, providing the structural basis of preferential conduction pathways and delivering the high ionic mobility crucial for the battery performance. A long-standing mystery exists between glasses and crystals of identical chemical composition when the vitreous counterparts usually exhibit the higher ionic conductivity.[9,10] This observation suggests differences in structural motifs for glasses and crystals, the latter are simply given by the phase diagram and crystal structure. Sodium thioarsenate binaries Na_2S-As_2S_3 belong to useful model systems to unravel this mystery since the two known ternary crystalline compositions, monoclinic $NaAsS_2$[11] and cubic Na_3AsS_3,[12] are congruently melting compounds[13] with contrasting network topology in addition to characteristic binary end-members, layered monoclinic orpiment[14] and/or triclinic anorpiment,[15] As_2S_3, and face-centered cubic Na_2S.[16] The 2D-layers of the both As_2S_3 polymorphs consist of 12-membered rings As_6S_6. Monoclinic metathioarsenate $NaAsS_2$ is built-up by corner-sharing pyramidal chains $(CS\text{-}AsSS_{2/2})_\infty$, held together by sodium cations, while in cubic orthothioarsenate Na_3AsS_3 the sodium species are connecting isolated pyramids AsS_3, Figure S1 in Supporting Information. A simple analogy with the equilibrium phase diagram would suggest a mixture of rings and chains for $(Na_2S)_x(As_2S_3)_{1-x}$ glasses at $x < 0.5$. Nevertheless, using time-of-flight neutron diffraction over a large range of the scattering vectors $Q = \frac{4\pi \sin\theta}{\lambda} \leq 40$ Å^{-1}, where 2θ is the scattering angle and λ the neutron wavelength, supported by first-principles molecular dynamics, we will show a structural and chemical diversity of sodium thioarsenate glasses at $x \leq 0.3$, not expected by a simple model.

2. MATERIALS AND METHODS

2.1. Synthesis. Glassy sodium thioarsenates, $(Na_2S)_x(As_2S_3)_{1-x}$, $0.0 \leq x \leq 0.3$, were obtained by direct synthesis of metallic sodium (Sigma-Aldrich, 99.9 %), sulfur pellets (Alfa Aesar, 99.999 %) and previously synthesized glassy arsenic sulfide placed in vitreous carbon crucibles in evacuated silica tubes (Figure S2 in Supporting information). The maximum synthesis temperature was 1150 K. The melts have homogenized at that temperature for 48-72h before quenching in water. The preparation procedures have been carried out in a glove box with controlled humidity. Other information related to temperature regimes and synthesis details can be found elsewhere.[17-19]

2.2. Neutron Diffraction Measurements. The synthesized sodium thioarsenate glasses were measured using time-of-flight neutron diffraction at the ISIS spallation neutron source (Rutherford Appleton Laboratory, UK). The GEM diffractometer[20] was used for these measurements at room temperature in vacuum-tight vanadium containers to avoid hydrogen contamination from atmospheric moisture. No impurity hydrogen signal was detected. The neutron diffraction data were corrected[21] for background and container scattering, multiple

scattering, self-attenuation, and inelasticity (Placzek) effects using the GUDRUN program[22] to obtain the total neutron structure factor $S_N(Q)$. A vanadium-niobium rod was also measured and used for data normalization.

2.3. First-Principles Simulations. Modeling of the neutron diffraction data was carried out using the Born-Oppenheimer molecular dynamics with the CP2K package.[23] The generalized gradient approximation and the PBEsol[24,25] or PBE0 hybrid[26,27] exchange-correlation functionals have been used. The employed first-principle molecular dynamics (FPMD) technique was similar to that used in previously published reports on chalcogenide glass systems.[28,29] The initial atomic configurations for glassy $(Na_2S)_{0.3}(As_2S_3)_{0.7}$ were created and optimized using the RMC_POT++ code[30,31] against the derived neutron structure factor of the sodium thioarsenate glass to obtain a good agreement with experimental data. The size of the cubic simulation box at room temperature, containing 440 atoms (60 Na, 140 As, and 240 S), was chosen to match the experimental number density. Further optimization has been carried using density functional theory (DFT), adopting for each atom involved the molecularly optimized correlation consistent polarized triple-zeta valence basis set TZVP[32,33] along with the Goedecker-Teter-Hutter (GTH) type pseudo-potentials.[34] The FPMD simulations after DFT optimization at 0 K were started at 300 K. In order to deal with a canonical NVT ensemble, a Nosé–Hoover[35,36] chain of length 3 has been employed as a thermostat. The PBEsol or PBE0 systems were heated above the glass transition temperature at 425 K up to 600 K using 100 K steps for 7 to 16 ps each. At 600 K, the systems were equilibrated for 20-23 ps and cooled down to 300 K using the same temperature steps and similar simulation time. Final equilibration and data collection at 300 K was done for 19-25 ps. The connectivity and ring statistics were analyzed using the R.I.N.G.S.[37] and modified connectivity[38] codes. For analysis of voids and cavities, the pyMolDyn[39] program was used.

3. RESULTS AND DISCUSSION

3.1. Reciprocal *Q*-Space. The derived neutron structure factors $S_N(Q)$ for $(Na_2S)_x(As_2S_3)_{1-x}$ glasses are shown in Figure 1. As expected, the first sharp diffraction peak (FSDP) at $Q_0 \approx 1.23$ Å^{-1} decreases with x; this is a typical behavior for alkali and d^{10} (Ag, Cu) cation-containing chalcogenide glasses.[40-43] The principle peak (PP) at $Q_1 \approx 2.4$ Å^{-1} increases in amplitude and shifts to lower scattering vectors Q while the second principle peak (PP2) at $Q_2 \approx 3.9$ Å^{-1} also shifts to lower Q decreasing the amplitude with x (Figure S3 in Supporting information). The high-Q oscillations, $Q \gtrsim 8$ Å^{-1}, remain essentially invariant.

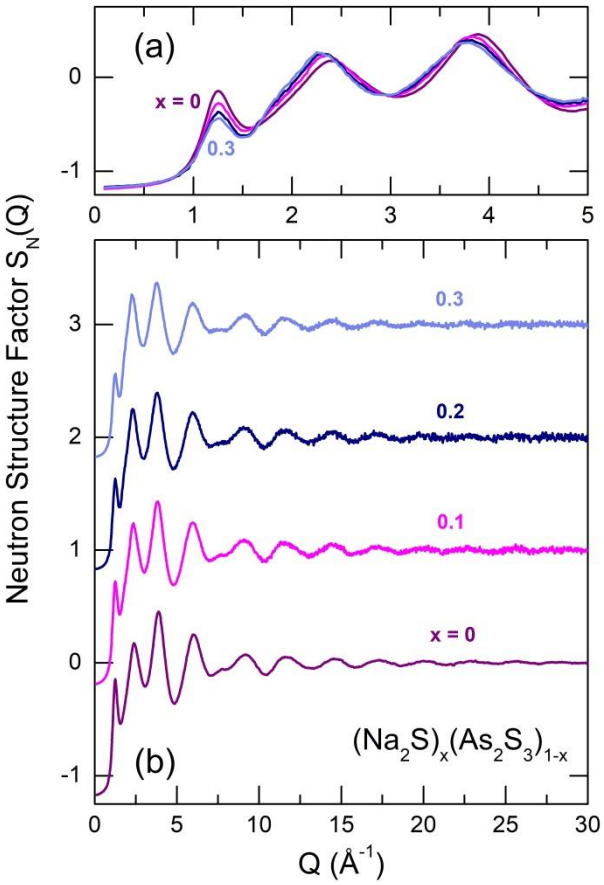

Figure 1. Neutron structure factors $S_N(Q)$ for $(Na_2S)_x(As_2S_3)_{1-x}$ glasses, $0 \le x \le 0.3$: (a) a low-Q part of the $S_N(Q)$, (b) the entire diffraction data with Q_{max} = 30 Å^{-1}.

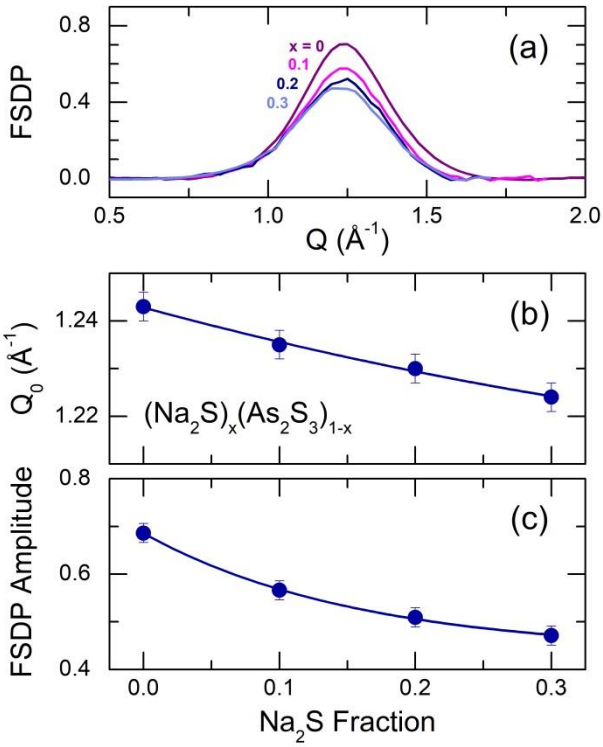

Figure 2. Compositional dependence of the first sharp diffraction peak: (a) isolated FSDPs, (b) the position Q_0, and (c) the FSDP amplitude as a function of x.

The FSDP was isolated using previously reported procedures[44,45] and shown in Figure 2(a). The observed monotonic shift, $\partial Q_0/\partial x = -0.077$ Å^{-1}, Figure 2(b), is markedly slower than that for PP and PP2, $\partial Q_1/\partial x \approx \partial Q_2/\partial x = -0.56 \pm 0.1$ Å^{-1}, Figure S3 (Supporting information), emphasizing a specific role of the FSDP in reflecting the intermediate range ordering of the As_2S_3 glassy host, in particular, a certain expansion and fragmentation. The last phenomenon is evidenced by a strongly decreasing glass transition temperature $T_g(x)$, Figure S4 in Supporting information, also a typical trend in metal-containing chalcogenide glasses. The increasing PP amplitude is often associated with the enhanced packing density in a glass[46] and repeatedly observed in high pressure studies.[47-49] Glassy $(Na_2S)_x(As_2S_3)_{1-x}$ exhibit a monotonic increase of the number density from 0.03902 atoms Å^{-3} (x = 0) to 0.04036 (x = 0.3), coherent with the above

observation, despite the apparent expansion of the glasses on the local and intermediate range scale, reflected by the negative derivatives $\partial Q_i/\partial x$.

3.2. Correlation Functions in r-Space. The neutron total correlation functions $T_N(r)$ obtained through the usual Fourier transform

$$T_N(r) = 4\pi\rho_0 r + \frac{2}{\pi}\int_0^{Q_{max}} Q[S_N(Q) - 1]\sin QrM(Q)\mathrm{d}Q\,, \quad (1)$$

using the Lorch[50] window function $M(Q)$, where ρ_0 is the number density and $Q_{max} = 30$ Å^{-1}, are shown in Figure 3.

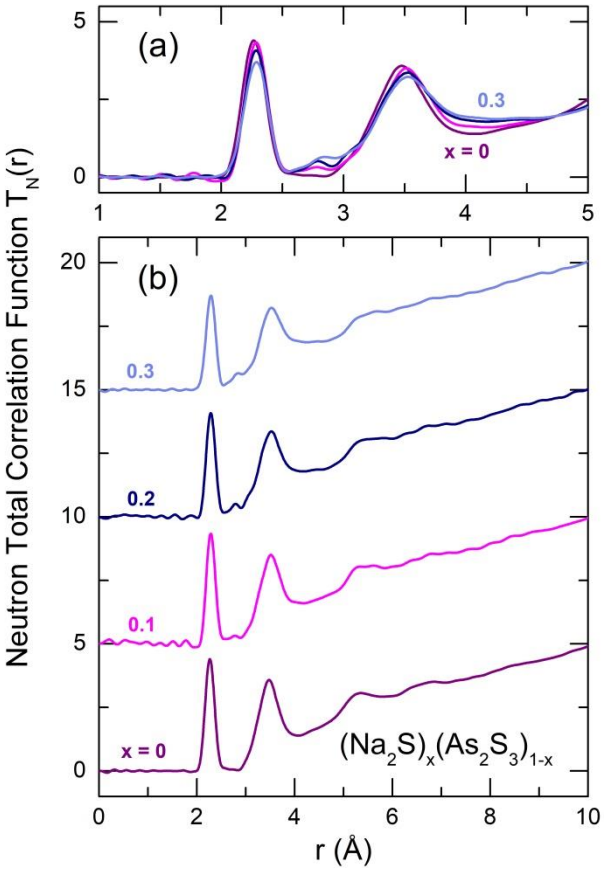

Figure 3. Neutron total correlation function $T_N(r)$ for $(Na_2S)_x(As_2S_3)_{1-x}$ glasses, $0 \le x \le 0.3$: (a) a low-r part of the $T_N(r)$, (b) the entire total correlation functions.

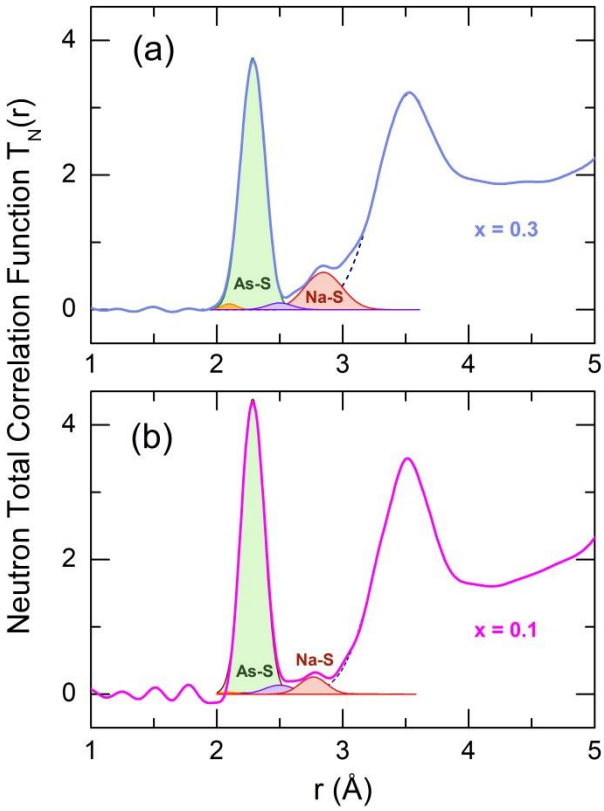

Figure 4. Typical fitting examples of $T_N(r)$ for (a) x = 0.3, and (b) x = 0.1 glasses. The S-S, As-S, As-As and Na-S NN correlations are highlighted in yellow, green, violet and light red, respectively.

The intense peak at 2.27 Å, corresponding to As-S nearest neighbors (NN), decreases with x following the stoichiometric relations, that is, the decreasing fraction of glassy As_2S_3. Instead, an emerging new feature appears and grows at ≈2.8 Å, related to Na-S NN contacts, as observed in crystalline sodium thioarsenates[11,12] and sodium sulfide glasses[42]. The As-S NN correlations are clearly shifted to higher r, Figure 3(a), producing network expansion on the local level. The second neighbor peak at ≈3.4 Å also shifts to higher r and broadens with increasing x. More importantly, the empty inter-pyramidal space in As_2S_3 glassy host, reflected by a minimum at 4 Å, is filling up with increasing sodium content, implying a higher packing density. The intermediate range structure of g-As_2S_3, characterized by distant correlations at 5.3 Å (a center-

center inter-pyramidal distance) and a broad feature at 6.5 Å, disappears progressively with x becoming nearly flat for glassy $(Na_2S)_{0.3}(As_2S_3)_{0.7}$.

Direct $T_N(r)$ fitting using Gaussians confirms the trigonal arsenic coordination, $2.86 \leq N_{As-S} \leq 2.91$, and suggests a tetrahedral sodium environment, $3.7 \leq N_{Na-S} \leq 4.0$. We should however note that fitting with symmetric functions does not necessarily exclude asymmetric coordination patterns for sodium and larger number of more distant nearest neighbors. Typical fittings are shown in Figure 4 taking glassy $(Na_2S)_{0.1}(As_2S_3)_{0.9}$ and $(Na_2S)_{0.3}(As_2S_3)_{0.7}$ as an example. The fitting results are summarized in Table 1.

A close inspection of $T_N(r)$ reveals that a three-peak fitting (As-S and Na-S NNs, and a second neighbor peak) is insufficient for both g-As_2S_3 and $(Na_2S)_x(As_2S_3)_{1-x}$. A weak peak at ≈2.08 Å and a distinct feature at ≈2.5 Å are particularly assumed, reflecting the presence of S-S and As-As homopolar bonds, also confirmed by S-S and As-As stretching frequencies in Raman spectra at 470-490 and ≈230 cm^{-1}, respectively (see Refs. [49,51,52] and Figure S5 in Supporting information). The observed chemical disorder $\chi = \frac{N_{As-As}}{N_{As-S}+N_{As-As}} = \frac{N_{S-S}}{N_{S-As}+N_{S-S}}$ is weak and hardly dependent on x, $0.02 \leq \chi \leq 0.04$, Table 1.

Table 1. Interatomic Distances r_{ij} and Local Coordination Numbers N_{ij} of Nearest Neighbors in Na_2S-As_2S_3 Glasses

Na_2S Fraction	r_{S-S} (Å)	N_{S-S}	r_{As-S} (Å)	N_{As-S}	r_{As-As} (Å)	N_{As-As}	r_{Na-S} (Å)	N_{Na-S}
0	2.04	0.03	2.264	2.90	2.54	0.05	–	–
0.1	a)	a)	2.285	2.86	2.52	0.11	2.77	4.0
0.2	2.08	0.04	2.285	2.90	2.51	0.05	2.82	3.9
0.3	2.10	0.10	2.287	2.91	2.50	0.08	2.84	3.7

a) the S-S nearest neighbor peak is too weak to be quantified reliably

3.3. First-Principles Molecular Dynamics. First-principles molecular dynamics (FPMD) using the generalized gradient approximation (GGA) with PBE or PBEsol functionals usually gives overestimated interatomic distances for chalcogenides and pnictides.[53,54] Modeling of $(Na_2S)_{0.3}(As_2S_3)_{0.7}$ is not an exception to the rule.

3.3.1. Comparison with Experiment and Partial Correlation Functions. The derived GGA/PBEsol neutron structure factor $S_N^{MD}(Q)$ reveals a systematic shift of medium- and high-Q oscillations to lower scattering vectors compared to experimental data, Figure 5, leading to larger distances in r-space, Figure S6 in Supporting information. The use of the hybrid exchange-correlation functional PBE0 combining the exact Hartree-Fock and DFT solutions[26,27] significantly improves the agreement both at high and low Q, similar to another hybrid B3LYP.[53] There are still some differences in the FSDP and PP shape, however, they are small and presumably related to insufficient size of the simulation box, 22.17 Å, for a fully adequate description of the intermediate-range order in a real glass. Similar behavior is often observed in FPMD modeling of glasses working with small boxes[55] because of heavy simulation costs.

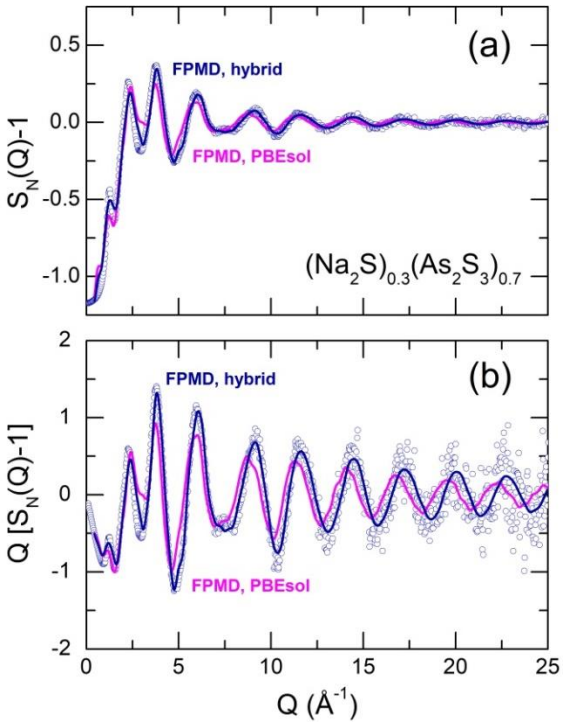

Figure 5. (a) Experimental neutron structure factor $S_N(Q) - 1$ and (b) interference function $Q[S_N(Q) - 1]$ for glassy $(Na_2S)_{0.3}(As_2S_3)_{0.7}$ (circles) and derived $S_N^{MD}(Q)$ related functions using GGA with PBEsol (magenta) and PBE0 (dark blue) functionals.

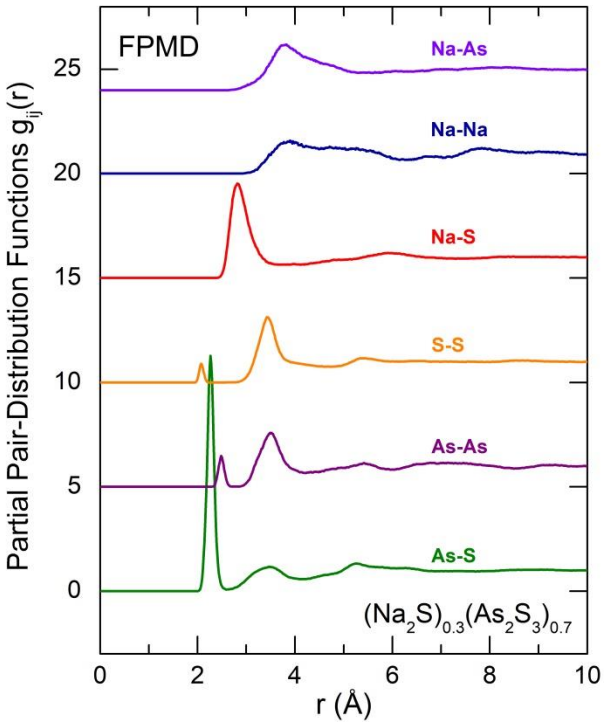

Figure 6. Derived FPMD GGA/PBE0 partial pair-distribution functions $g_{ij}(r)$ for Na-As (violet), Na-Na (dark blue), Na-S (red), S-S (orange), As-As (purple), and As-S (green) atomic pairs.

The GGA/PBE0 partial structure factors $S_{ij}(Q)$ are given in Figure S7 (Supporting information). Similar to glassy As_2S_3,[56,57] we note that the origin of the FSDP comes from As-As and to some extent from As-S correlations. The principal peaks of the Na-Na and Na-As partials are responsible for emerging asymmetry of the experimental PP in the vicinity of 1.8 Å^{-1}, Figure 1(a). We should also note a distinct low-Q peak at 0.7 Å^{-1} in $S_{NaNa}(Q)$ reflecting some intermediate range ordering of sodium cations.

The full set of GGA/PBE0 partials $g_{ij}(r)$ is shown in Figure 6. As expected, the As-S correlations are predominant in the experimental 2.28 Å peak, while their Na-S counterparts represent the main component of the 2.8 Å peak, Figure 3(a). The S-S and As-As real-space partials exhibit first-neighbor correlations at 2.07 and 2.48 Å, respectively, indicating a chemical disorder χ in glassy $(Na_2S)_{0.3}(As_2S_3)_{0.7}$. The derived χ-value, χ^{MD} = 0.06, is slightly higher than the experimental result, χ = 0.04±0.01, Table 1.

3.3.2. Arsenic, Terminal Sulfur and Sodium Coordination. The partial coordination numbers for arsenic, sulfur and sodium are given in Figures 7 and 8. The trigonal arsenic coordination is clearly dominant; 98.4 % of As species have three sulfur and/or arsenic nearest neighbors, determined using the cutoff distance of 2.62 Å, corresponding to a sharp minimum at the partial pair-distribution function $g_{AsS}(r)$, Figure 6. The fraction of dissimilar (S) and alike (As) NNs for the central arsenic atom is shown in the inset in the form of $As(S_{3-m}As_m)$ statistics. The AsS_3 pyramids (m = 0) appear to be the majority entities (80 %); the observed chemical disorder is reflected by 19 % of pyramidal units with As-As homopolar bond (m = 1).

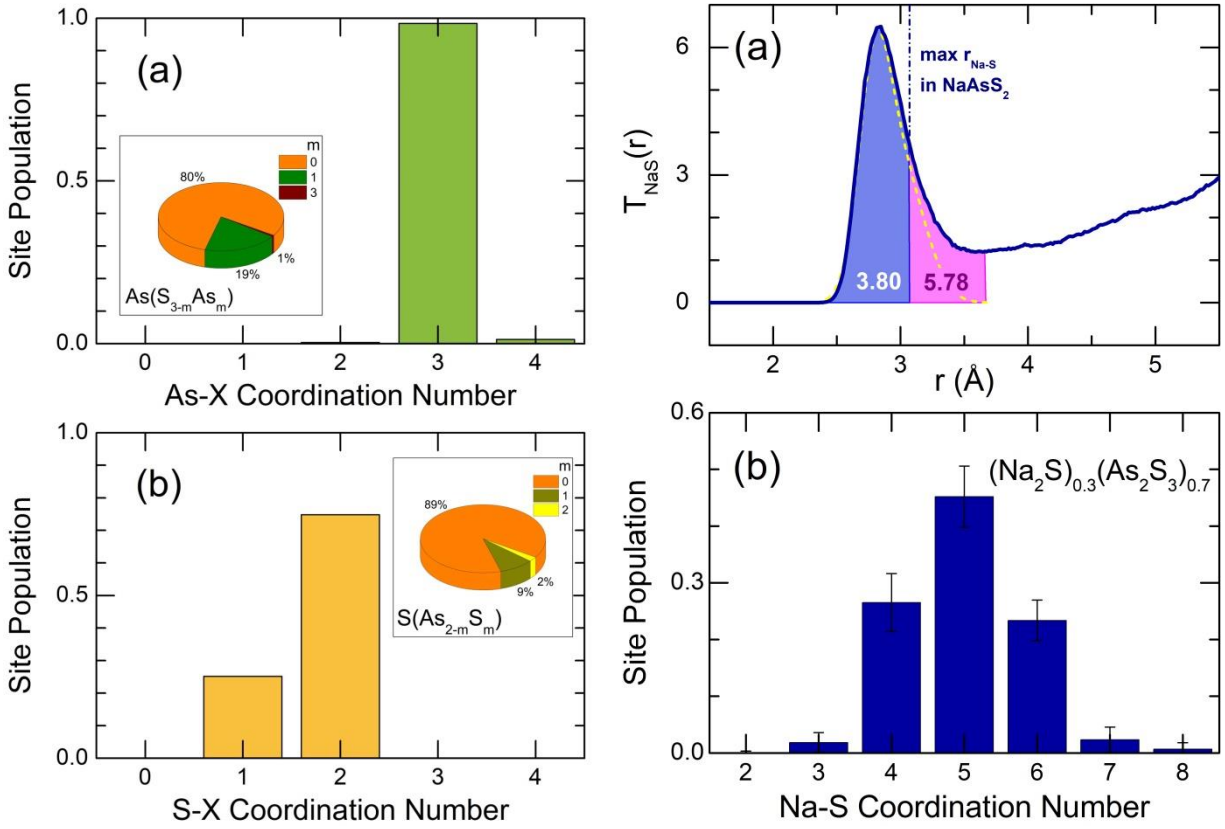

Figure 7. Partial coordination numbers for (a) arsenic, $N_{\mathrm{As-X}}$, and (b) sulfur, $N_{\mathrm{S-X}}$, where X = As or S, integrated using the cutoff distance of 2.62 Å, corresponding to a sharp minimum at $g_{\mathrm{AsS}}(r)$. The insets show the NN distributions for central atoms in trigonal (As) or two-fold (S) local coordination as the fraction of alike atoms m for As, As($S_{3-m}As_m$) and S, S($As_{2-m}S_m$).

Figure 8. (a) Partial correlation function $T_{\mathrm{NaS}}(r)$ with two different cutoffs: 3.07 Å, related to the maximum Na-S distance in monoclinic $NaAsS_2$, and 3.67 Å, corresponding to a flat minimum at $g_{\mathrm{NaS}}(r)$; the numbers indicate the $N_{\mathrm{Na-S}}$ value for each cutoff; and (b) distribution of partial coordination numbers for sodium, determined using the cutoff distance of 3.35 Å. See text for further details.

The sulfur local coordination is $N_{\mathrm{S-X}}$ = 1.75, where X = As or S. We note that $N_{\mathrm{S-X}}$ is the partial coordination number, related only to S-As or S-S atomic pairs. The two-fold sulfur coordination is predominant (74.8 %). The population of terminal sulfur S(t), $N_{\mathrm{S-As}}$ = 1, is by a factor of 3 smaller, 23.6 %, and almost corresponds to the expected value of 25 %, following a simple stoichiometric relation $Na_2S + As_2S_3 = 2AsS(t)S(b)_{2/2}^{-} + 2Na^{+}$, where S($b$) corresponds to bridging sulfur, $N_{\mathrm{S-As}}$ = 2.

Calculating the sodium local coordination is less straightforward since the $g_{\mathrm{NaS}}(r)$ partial pair-distribution function has a long tail at high r without a well-defined minimum, Figure 6. Figure 8(a) reveals several approaches. (1) Taking the maximum Na-S interatomic distance in monoclinic $NaAsS_2$, $r_{\mathrm{Na-S}}^{\mathrm{max}}$ = 3.07 Å,[11] as a cutoff, the Na-S coordination number appears to be $N_{\mathrm{Na-S}}$ = 3.80. (2) A direct fitting of $T_{\mathrm{NaS}}(r)$ with three Gaussians reproduces well the asymmetric shape of the partial Na-S correlation function below 4 Å, assuming the first two peaks at 2.79 and 3.00 Å represent the Na-S NN contacts, while the third one at 3.65 Å is related to the second neighbors. The dashed yellow line in Figure 8(a) shows the sum of the two NN contributions and yields $N_{\mathrm{Na-S}}$ = 4.55. (3) Finally, a conservative approach, taking a shallow minimum in $g_{\mathrm{NaS}}(r)$ at 3.67A as a cutoff, results in $N_{\mathrm{Na-S}}$ = 5.78 (the integrated area highlighted in magenta). Resuming these three scenarios, one can conclude:

- the average Na-S coordination number $\langle N_{\mathrm{Na-S}} \rangle$ is below six;
- some distant Na-S contacts, $3.1 \lesssim r_{\mathrm{Na-S}} \lesssim 3.7$ Å, seem to be the second neighbor correlations similar to Na-As and Na-Na atomic pairs, which exhibit a non-negligible population over the indicated r-range, Figure 6;
- the best estimate of the average Na-S NN coordination is $4.5 \leq \langle N_{\mathrm{Na-S}} \rangle \leq 5.5$.

A wide distribution of the local Na-S coordination numbers, corresponding to the cutoff distance of 3.35 Å and $\langle N_{\mathrm{Na-S}} \rangle$ = 5, is shown in Figure 8(b). We note a nearly symmetric distribution centered at $N_{\mathrm{Na-S}}$ = 5 and two comparable fractions of 4- and 6-fold coordinated sodium.

3.3.3. Angular Distributions. The selected bond angle distributions $B(\theta)$ are summarized in Figure 9. The S-As-S angle distribution is almost symmetric, centered at 97.8°. The geometry of AsS_3 pyramidal units is similar to that in monoclinic As_2S_3[14] and $NaAsS_2$,[11] evidenced by respective $B(\theta_{\mathrm{SAsS}})$. In contrast, the pyramidal connectivity, reflected by $B(\theta_{\mathrm{AsSAs}})$, is variable showing three major contributions at 89°, 101° and 120°, highlighted in Figure 9(b) in different colors. The crystalline As_2S_3 and $NaAsS_2$ pyramidal connectivity, also shown in Figure 9(b), only partially reproduces that in glassy $(Na_2S)_{0.3}(As_2S_3)_{0.7}$. The high-angle contribution, $\langle \theta_{\mathrm{AsSAs}} \rangle$ = 120°, is missing in crystals.

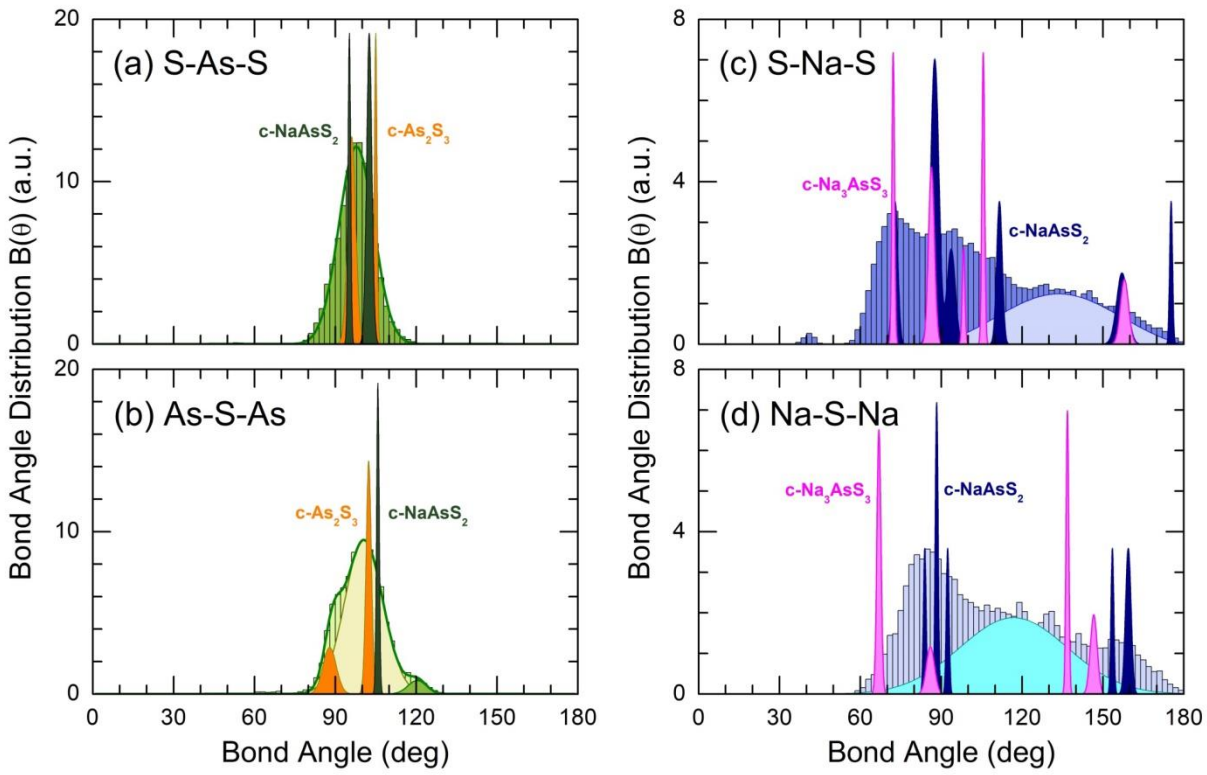

Figure 9. Selected bond angle distributions $B(\theta)$ for glassy $(Na_2S)_{0.3}(As_2S_3)_{0.7}$: (a) S-As-S, (b) As-S-As, (c) S-Na-S, and (d) Na-S-Na. The crystal data for monoclinic As_2S_3,[14] monoclinic $NaAsS_2$,[11] and cubic Na_3AsS_3[12] are also shown. The fitting results for $B(\theta_{\mathrm{AsSAs}})$, $B(\theta_{\mathrm{SNaS}})$, and $B(\theta_{\mathrm{NaSNa}})$ are highlighted in different colors (see text for further details).

The sodium-related $B(\theta_{\mathrm{SNaS}})$ and $B(\theta_{\mathrm{NaSNa}})$ distributions are spread over a large angular range, $30° \leq \theta_{\mathrm{SNaS}} \leq 180°$ and $50° \leq \theta_{\mathrm{NaSNa}} \leq 180°$, respectively, both in glassy $(Na_2S)_{0.3}(As_2S_3)_{0.7}$ and crystalline sodium thioarsenates. Basically, the geometry of Na-S polyhedra in the glass is reminiscent of that in monoclinic $NaAsS_2$[11] and cubic Na_3AsS_3,[12] Figure 9(c). However, a weak

contribution at low angles, $\langle\theta_{SNaS}\rangle = 41°$, and a significant broad component at high-θ, $\langle\theta_{SNaS}\rangle$ = 134±2°, highlighted in light blue, Figure 9(c), are observed only for glassy $(Na_2S)_{0.3}(As_2S_3)_{0.7}$. The connectivity of Na-S polyhedra is rather similar to that in monoclinic $NaAsS_2$ but also only partially. A broad contribution at medium Na-S-Na angles, $\langle\theta_{NaSNa}\rangle$ = 117±2°, highlighted in cyan in Figure 9(d), is missing in crystals.

3.3.4. Rings, Chains and Cavities. Glassy As_2S_3 is characterized by a quasi-continuous disordered network; 97 % of arsenic and sulfur species are connected into a single piece. Sodium thioarsenate glasses have a fragmented host matrix evidenced by a strongly decreased glass transition temperature, Figure S4. In glassy $(Na_2S)_{0.3}(As_2S_3)_{0.7}$, just two-thirds of As and S form a single connected fragment, the remaining species are either isolated or building-up small clusters: pyramidal units AsS_3, corner- and edge-sharing oligomeric chains, connected together by sodium, Figure 10.

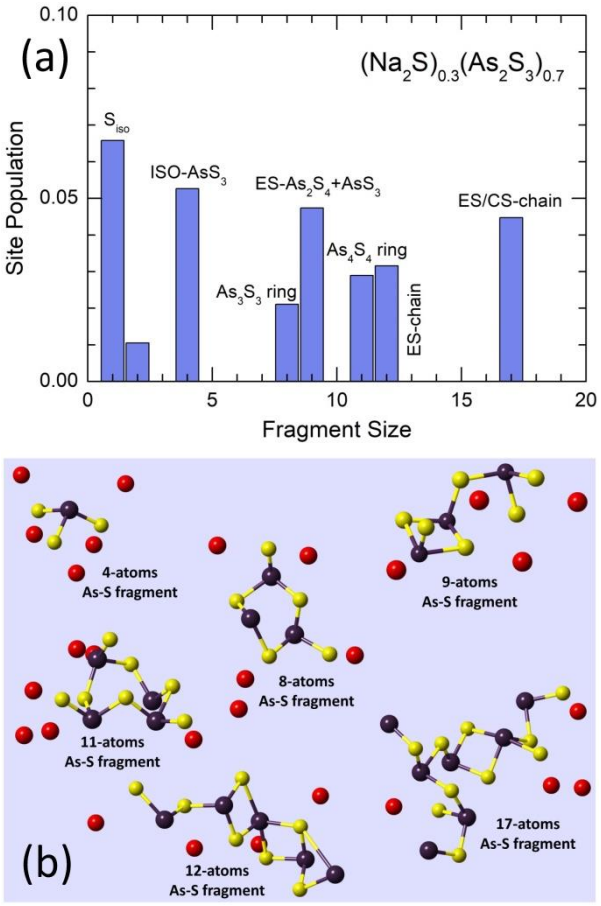

Figure 10. Small As-S fragments forming a disconnected As-S subnetwork in g-$(Na_2S)_{0.3}(As_2S_3)_{0.7}$: (a) statistics of small As-S units, and (b) typical examples present in the FPMD simulation box.

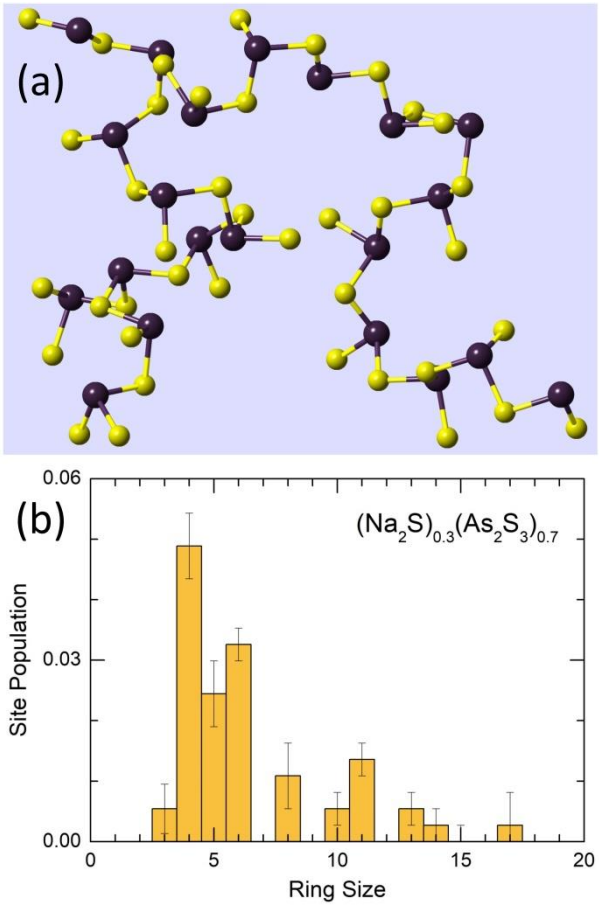

Figure 11. (a) 60-atoms long As-S chain consisting of corner-sharing pyramidal units CS-$AsS_{3/n}$, where n = 1, S(t), or 2, S(b), and (b) the derived ring statistics in glassy $(Na_2S)_{0.3}(As_2S_3)_{0.7}$.

The topology of the connected fragment in $(Na_2S)_{0.3}(As_2S_3)_{0.7}$, is also different from that in glassy As_2S_3. The latter is almost exclusively composed of As_pS_q rings, where $p \approx q$ and $3 \le p+q \le 35$,[49,57] while the former represents a mixture of chains (57 %) and rings (43 %). The derived ring statistics is shown in Figure 11(b) and mostly characterized by small rings, $p+q \le 11$, while the chains are long and essentially consist of corner-sharing pyramids CS-$AsS_{3/n}$ with terminal sulfur S(t), n = 1, and bridging sulfur S(b), n = 2, Figure 11(a).

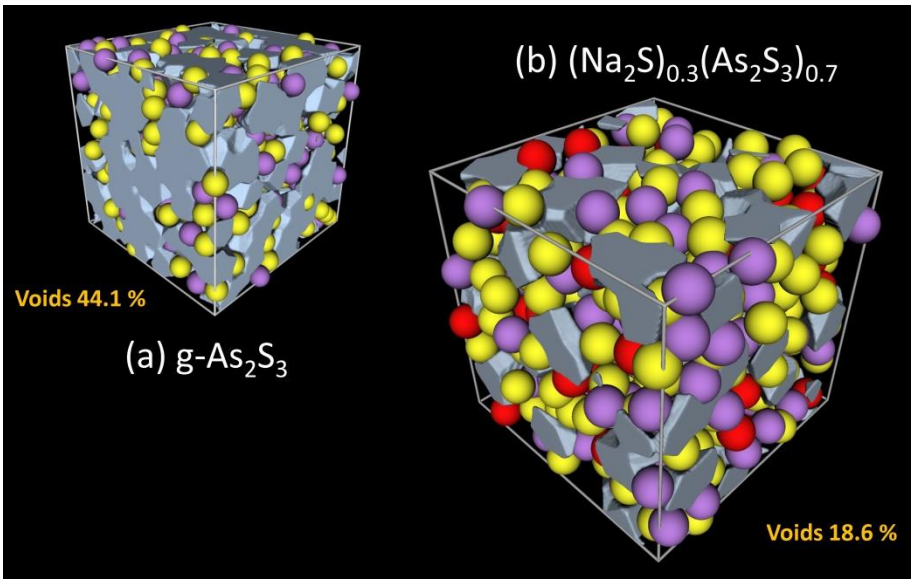

Figure 12. Cavities in (a) g-As_2S_3[49] and (b) g-$(Na_2S)_{0.3}(As_2S_3)_{0.7}$, derived using the pyMolDyn program.[39] The fraction of voids normalized to the simulation box volume has decreased by a factor of 2.4, from 44.1 % to 18.6 %, for the sodium thioarsenate glass.

The enhanced amplitude of the principle peak at $Q_1 \approx 2.4$ Å^{-1} with increasing sodium content, Fig. 1, suggests higher packing density in sodium thioarsenate glasses, confirmed by macroscopic number density. Similar conclusion can be drawn calculating the volume of microscopic cavities in $(Na_2S)_{0.3}(As_2S_3)_{0.7}$ by pyMolDyn code,[39] applying Dirichlet–Voronoi constructions and using the atomic positions and a cutoff radius of the test particle, 2.6 Å in our case. The results, shown in Figure 12, indicate a significant decrease of the total volume of voids, normalized to the size of the FPMD simulation box, from 44.1 % in glassy As_2S_3[49] to 18.6 % for glassy sodium thioarsenate. This trend was observed earlier in silver thioarsenate and thiogermanate glasses[58,59] and represents a typical behavior for metal chalcogenide glasses.

3.3.5. Isolated Sulfur. A small part of sulfur does not have arsenic nearest neighbors; we will call them isolated sulfur S_{iso}. The fraction of isolated sulfur was found to be S_{iso}/S_{total} = 6.2 %, and these species are only bound to sodium, Figure 13. The origin of isolated sulfur in crystalline ternary and more complex metal sulfides is directly related to stoichiometric relations and coordination constraints. The cubic lattice of argyrodite $Ag_8GeS_6 = 4Ag_2S{\cdot}GeS_2$ contains ⅓ of isolated sulfur and ⅔ of sulfur in GeS_4 tetrahedra, all connected by silver.[60] In glassy silver and thallium thiogermanates and thioarsenates, the isolated sulfur species appear far below the expected limits, $M_2S/GeS_2 = 2$ and $M_2S/As_2S_3 = 3$, and in substantial concentrations, $0.21 \le S_{iso}/S_{tot} \le 0.28$, for x = 45-50 mol.% M_2S.[61] Likewise, the FPMD modeling of equimolar $(Na_2S)_{0.5}(GeS_2)_{0.5}$ glass[62] has shown the presence of 23.5 % of isolated sulfur. In average, each isolated sulfur species is connected to two neighboring cations, $M/S_{iso} \cong 2$, and together they form broad pathways going through the entire simulation box and ensuring high ionic conductivity, Figure S8 (Supporting Information).[61] This characteristic pattern is not yet reached in glassy $(Na_2S)_{0.3}(As_2S_3)_{0.7}$. The connectivity analysis of sodium distribution $P_{\mathrm{NaNa}}(r)$ shows, Figure 13(c), that the average Na-Na separation distance over the entire simulation box is centered at 4.5 Å for more than 70 % of sodium, while the most frequent Na-Na contacts between Na-S_{iso} units occur at 6.7 Å (> 50 % of the sodium species involved). In other words, the Na-S_{iso} units are still far away from each other and do not contribute substantially to the Na^+ ion

transport, consistent with low sodium conductivity in glassy $(Na_2S)_{0.3}(As_2S_3)_{0.7}$, 2×10^{-11} S cm^{-1} at room temperature, Figure S9 (Supporting Information), also characterized by high activation energy, E_a = 0.80±0.04 eV, compared to $(Na_2S)_{0.33}(GeS_2)_{0.67}$ glasses, 7×10^{-8} S cm^{-1} and 0.54 eV.[10] This finding is coherent with significant population of S_{iso} species in glassy sodium thiogermanates[62] mentioned above.

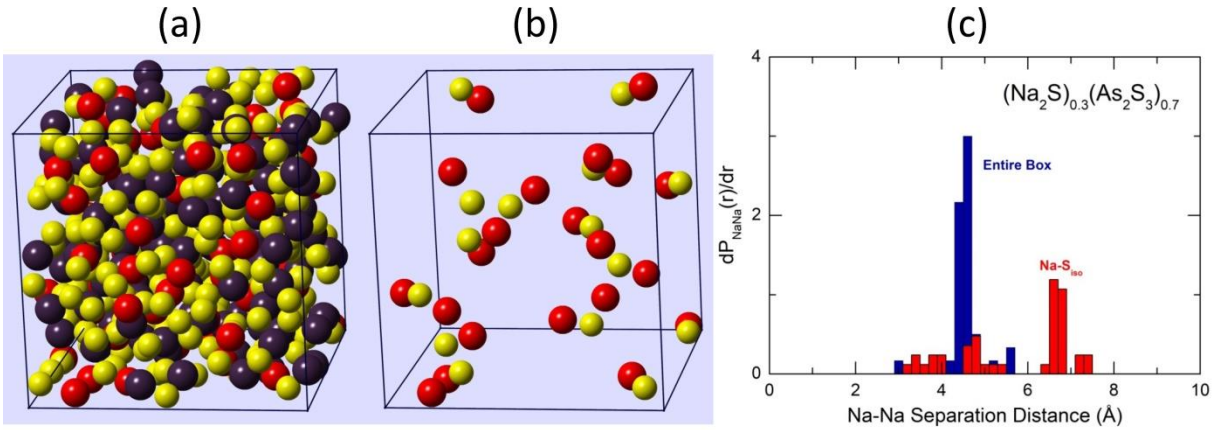

Figure 13. Isolated sulfur in glassy $(Na_2S)_{0.3}(As_2S_3)_{0.7}$: (a) the entire FPMD simulation box containing 440 atoms (60 Na, 140 As, 240 S), (b) isolated sulfur species with connected sodium cations, and (c) the average Na-Na separation distances for the entire box (blue) and Na-S_{iso} connected fragments (red).

3.4. Chemical and Structural Variety in Sodium Thioarsenate Glasses. The FPMD results indicate that glassy $(Na_2S)_{0.3}(As_2S_3)_{0.7}$ exhibits complicated chemical and structural trends compared to the expected behavior suggested by the equilibrium phase diagram Na_2S-As_2S_3.[13] Two ternary compounds were reported in this system in addition to the binary end members: monoclinic orpiment/triclinic anorpiment As_2S_3[14,15] and face-centered cubic Na_2S.[16] Monoclinic metathioarsenate $NaAsS_2$ (x = 0.5) consists of corner-sharing chains CS-$(AsSS_{2/2})_\infty$,[11] while cubic orthothioarsenate Na_3AsS_3 (x = 0.75) is built-up by AsS_3 pyramids;[12] the As-S entities are connected by sodium. Taking into account the sodium content in glassy $(Na_2S)_{0.3}(As_2S_3)_{0.7}$, one would expect fragmented domains containing As_pS_q rings (57 %) and CS-$(AsSS_{2/2})_k$ chains with neighboring Na species (43 %). The simulated network differs both chemically and structurally from these expectations. First, Na_2S_{iso} monomers, AsS_3 pyramids and ES-As_2S_4 clusters with connected sodium species appear to be unexpected chemical varieties, absent in the equilibrium phase diagram for this particular composition or completely. In addition to the expected CS-$(AsSS_{2/2})_k$ chains or chain fragments, the cross-linking entities, edge-sharing or mixed edge/corner-sharing oligomers were observed, Figure 10. Finally, the As_pS_q ring statistics changes considerably compared to crystalline and glassy As_2S_3, unveiling the dominance of small rings and the absence of 12-fold entities (crystalline As_2S_3) or large varieties, $14 \le p+q \le 35$ (glassy As_2S_3), Figure S10 in Supporting information. The observed characteristic features and unexpected differences are consistent with our Raman study of $(Na_2S)_x(As_2S_3)_{1-x}$ glasses supported by DFT modeling, Figure S11, to be published elsewhere.

In spite of rather low sodium content in glassy $(Na_2S)_{0.3}(As_2S_3)_{0.7}$, 13.6 at.% Na, the sodium related partial pair-distribution functions also show unusual trends. To some extent, they are even reminiscent of sodium-rich orthothioarsenate Na_3AsS_3 (x = 0.75, 42.9 at.% Na). In particular, the $g_{\mathrm{NaNa}}(r)$ exhibits a low-r tail between $3.1 \le r_{\mathrm{NaNa}} \le 3.6$ Å, Figure 14(c), also visible in Figure 13(c). The shortest Na-Na correlations in monoclinic $NaAsS_2$ (25 at.% Na) occur

only at 4.0 Å, while cubic Na_3AsS_3 reveals short Na-Na contacts at 3.4 Å. In other words, sodium in g-$(Na_2S)_{0.3}(As_2S_3)_{0.7}$ starts to show a non-random distribution with Na-rich domains. At higher x, these domains would be connected and yield preferential conduction pathways with high ionic mobility explaining faster ionic transport in glasses compared to crystalline counterparts with comparable mobile cation content. The last phenomenon is well known for vitreous and crystalline ion conductors.[9,10]

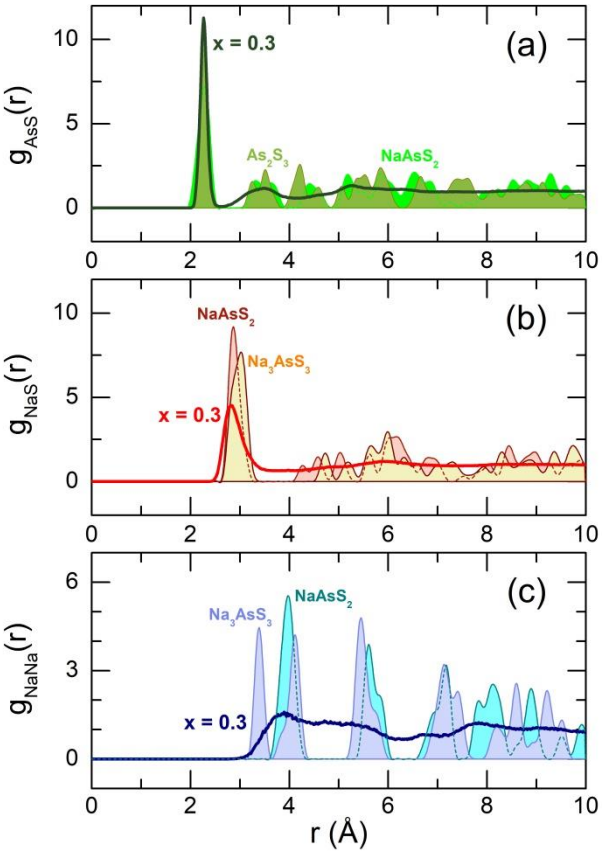

Figure 14. Partial pair-distribution functions in glassy $(Na_2S)_{0.3}(As_2S_3)_{0.7}$ in comparison with crystalline references: (a) $g_{AsS}(r)$, (b) $g_{NaS}(r)$, and (c) $g_{NaNa}(r)$. The data for monoclinic As_2S_3[14] and $NaAsS_2$,[11] and cubic Na_3AsS_3[12] were calculated from the cif files using the XTAL program.[63]

A wide distribution of the Na-S second neighbor correlations in glassy $(Na_2S)_{0.3}(As_2S_3)_{0.7}$, Figure 14(b), mentioned previously in connection to uncertainty in determining the local Na-S NN coordination number, indicates a fairly disordered nature of Na-S contacts. A strong sodium-related disorder is also seen for $g_{NaNa}(r)$, Figure 14(c). The two Na-S and Na-Na partial functions do not reveal a clear distinction between different coordination shells opposite to the crystals, where the first and second Na-S neighbors are well defined, Figure 14(b). In contrast, the first and second As-S neighbors are definitely distinguishable in glasses despite the inherent disorder and comparable with those in monoclinic As_2S_3 and $NaAsS_2$, Figure 14(a).

A drastic difference in structural disorder between As-S and Na-S subnetworks is also visible in angular dependences $B(\theta)$, Figure 9, and local coordination distributions, Figures 7 and 8. First, the geometry of AsS_3 pyramidal units in glasses is just a disorder-driven broadening of the crystalline parameters. In contrast, the Na-S polyhedra exhibit some shapes atypical for crystals, whose population reaches 38 %, estimated as the fraction of the bond angles centered at θ_{SNaS} = 134° to the total area of the S-Na-S angular envelope, Figure 9(c). Atypical connectivity of AsS_3

pyramids is small, 3.6±0.4 %, deduced as the fraction of As-S-As angles centered at 120°, Figure 9(b). In opposite, roughly half of the Na-S polyhedral connections do not occur in crystalline references, Figure 9(d).

The trigonal arsenic coordination is well preserved in both glasses and crystals. The sodium coordination in crystalline thioarsenates is six;[11,12] binary Na_2S has tetrahedral sodium environment.[16] The dominant Na-S coordination number in glassy $(Na_2S)_{0.3}(As_2S_3)_{0.7}$ is N_{Na-S} = 5 (45±5 %), tetrahedral (27 %) and octahedral (23 %) sodium species appear to be the minority entities, Figure 8(b).

Compared to the reported FPMD studies of sodium and lithium sulfide glasses, we note some common trends and differences. A wide range of characteristic structural motifs was also found in $(Na_2S)_x(P_2S_5)_{1-x}$ glasses, $0.33 \le x \le 0.75$, consisting of 8 entities,[64] confirmed independently by Raman, infrared and ^{31}P MAS NMR spectroscopy.[65] On the contrary, the reported crystalline references, $Na_2P_2S_6$,[66] $Na_4P_2S_6$,[66] and Na_3PS_4,[67,68] provide only three typical phosphorus environments; the remaining units observed in glasses appear to be metastable. The isolated sulfur species S_{iso} were reported in sodium thiogermanate glasses;[62] the equimolar composition $(Na_2S)_{0.5}(GeS_2)_{0.5}$ contains 23.5 % of S_{iso}, far below the stoichiometric crystal limit of Na_2S/GeS_2 = 2 (x = 0.67). In contrast, a FPMD study of vitreous Li_2S-P_2S_5 alloys[60] shows the appearance of isolated sulfur only above Li_2S/P_2S_5 = 3 in accordance with crystal data. We are planning to continue our FPMD modeling on similar sodium thiogallate and thiogermanate systems to obtain more information for these interesting and practically important glasses.

4. CONCLUSIONS

Pulsed neutron diffraction of sodium thioarsenate glasses Na_2S-As_2S_3 supported by first-principles simulations using a hybrid GGA/PBE0 exchange-correlation functional has shown multiple characteristic trends:

- fragmentation of a quasi-continuous As_2S_3 glassy host (97 % of connected As and S) into a fragmented network consisting of small disconnected As-S entities (≈⅓ of As and S) and a large connected subnetwork (the remaining two thirds), built-up by small rings As_pS_q, p+$q \le 11$, and long corner-sharing pyramidal chains CS-$(AsS_{3/n})_k$ with bridging S(b), n = 2, and terminal S(t), n = 1, sulfur species, all connected by neighboring Na cations; the fragmentation is evidenced macroscopically (a monotonic decrease of the glass transition temperature) and on the intermediate range scale (a FSDP reduction);
- the dominant trigonal arsenic local coordination remains intact while a wide distribution of the Na-S nearest neighbors, $3 \le N_{Na-S} \le 7$, centered at the average sodium coordination $\langle N_{Na-S} \rangle$ = 5, is observed;
- the derived structural motifs are different, both topologically and chemically, from the expected ones, related to vitreous As_2S_3 and sodium metathioarsenate $NaAsS_2$, revealing sodium-rich domains evidenced by the $g_{NaNa}(r)$ partial function, and also including a small fraction of binary units Na_2S_{iso}, 6.2 % of total sulfur;
- the binary units are still far away from each other, 6-7 Å in average, in contrast to superionic silver sulfide glasses, where preferential conduction pathways are formed by

directly connected Ag_2S_{iso} entities, explaining low ionic conductivity of glassy $(Na_2S)_{0.3}(As_2S_3)_{0.7}$, 2×10^{-11} S cm^{-1} at room temperature.

ASSOCIATED CONTENT

Supporting Information

The Supporting Information is available free of charge at …

Characteristic structural motifs in crystalline references; pictures of synthesized materials in the Na_2S-As_2S_3 system; additional neutron diffraction data; additional FPMD data; glass transition temperatures of sodium thioarsenate glasses; additional Raman and DFT data; preferential conduction pathways in silver thiogermanate glasses and ^{110m}Ag tracer diffusion; conductivity temperature dependences; ring statistics in glassy and crystalline As_2S_3.

AUTHOR INFORMATION

Corresponding Author

Eugene Bychkov – *Laboratoire de Physico-Chimie de l'Atmosphère, Université du Littoral Côte d'Opale, 59140 Dunkerque, France*; orcid: 0000-0002-3292-1205; Phone: +33 328 658250; Email: bychkov@univ-littoral.fr; FAX: +33 328 658244

Authors

Mohammad Kassem – *Laboratoire de Physico-Chimie de l'Atmosphère, Université du Littoral Côte d'Opale, 59140 Dunkerque, France*; orcid: 0000-0003-0512-0004; Email: mohamad.kassem@univ-littoral.fr

Tinehinane Bounazef – *Laboratoire de Physico-Chimie de l'Atmosphère, Université du Littoral Côte d'Opale, 59140 Dunkerque,* Email: tinehinane.bounazef@univ-littoral.fr

Daniele Fontanari – *Laboratoire de Physico-Chimie de l'Atmosphère, Université du Littoral Côte d'Opale, 59140 Dunkerque,* Email: danielefontanari@gmail.com

Anton Sokolov – *Laboratoire de Physico-Chimie de l'Atmosphère, Université du Littoral Côte d'Opale, 59140 Dunkerque,* Email: anton.sokolov@univ-littoral.fr

Maria Bokova – *Laboratoire de Physico-Chimie de l'Atmosphère, Université du Littoral Côte d'Opale, 59140 Dunkerque,* orcid: 0000-0002-2419-1644, Email: maria.bokova@univ-littoral.fr

Alex C. Hannon – *ISIS Facility, Rutherford Appleton Laboratory, Chilton, Didcot, OX11 0QX, U.K.*, orcid: 0000-0001-5914-1295; Email: alex.hannon@stfc.ac.uk

Notes

The authors declare no competing financial interest.

ACKNOWLEDGMENTS

This work was supported by the Région Hauts de France and the Ministère de l'Enseignement Supérieur et de la Recherche (CPER Climibio) as well as by the European Fund for Regional Economic Development. Work at the ISIS spallation neutron source (Rutherford Appleton Laboratory) was done within the proposal RB1820299 supported by the U. K. Science and Technology Facilities Council. The FPMD simulations were carried out using the CALCULCO computing platform, supported by SCoSI/ULCO (Service COmmun du Système d'Information de l'Université du Littoral Côte d'Opale). This work was also granted access to the HPC resources of IDRIS under the allocations 2018-A0050910639 and 2019-A0070910639 made by GENCI (Grand Equipement National de Calcul Intensif).

REFERENCES

(1) Goodenough, J. B. Rechargeable Batteries: Challenges Old and New. *J. Solid State Electrochem*. **2012**, *16*, 2019–2029.

(2) Hayashi, A.; Noi, K.; Sakuda, A.; Tatsumisago, M. Superionic Glass-Ceramic Electrolytes for Room-Temperature Rechargeable Sodium Batteries. *Nature Commun*. **2012**, *3*, 856.

(3) Chu, I.-H.; Kompella, C. S.; Nguyen, H.; Zhu, Z.; Hy, S.; Deng, Z.; Meng, Y. S.; Ong, S. P. Room-Temperature All-Solid-State Rechargeable Sodium-Ion Batteries with a Cl-doped Na_3PS_4 Superionic Conductor. *Sci. Reports* **2016**, *6*, 33733.

(4) Banerjee, A.; Park K. H.; Heo, J. W.; Nam, Y. J.; Moon, C. K.; Oh, S. M.; Hong, S.-T.; Jung, Y. S. Na_3SbS_4: A Solution Processable Sodium Superionic Conductor for All-Solid-State Sodium-Ion Batteries. *Angew. Chem. Int. Ed*. **2016**, *55*, 9634–9638.

(5) Chi, X.; Liang, Y.; Hao, F.; Zhang, Y.; Whiteley, J.; Dong, H.; Hu, P.; Lee, S.; Yao, Y. Tailored Organic Electrode Material Compatible with Sulfide Electrolyte for Stable All-Solid-State Sodium Batteries. *Angew. Chem. Int. Ed*. **2018**, *57*, 2630–2634.

(6) Kato, Y.; Hori, S.; Saito, T.; Suzuki, K.; Hirayama, M.; Mitsui, A.; Yonemura, M.; Iba, H.; Kanno, R. High-Power All-Solid-State Batteries using Sulfide Superionic Conductors. *Nature Energy* **2016**, *1*, 16030.

(7) Nishimura, S.-I.; Tanibata, N.; Hayashi, A.; Tatsumisago, M.; Yamada, A. The Crystal Structure and Sodium Disorder of High Temperature Polymorph β-Na_3PS_4. *J. Mater. Chem. A* **2017**, *5*, 25025–25030.

(8) Hayashi, A.; Masuzawa, N.; Yubuchi, S.; Tsuji, F.; Hotehama, C.; Sakuda, A.; Tatsumisago, M.; A Sodium-Ion Sulfide Solid Electrolyte with Unprecedented Conductivity at Room Temperature. *Nature Commun*. **2019**, *10*, 5266.

(9) Angell, C. A. Fast Ion Motion in Glassy and Amorphous Materials. *Solid State Ionics* **1985**, *9–10*, 3–16.

(10) Pradel, A.; Ribes M. Ionic Conductivity of Chalcogenide Glasses. In *Chalcogenide Glasses: Preparation, Properties and Applications*; Adam, J.-L., Zhang, X., Eds.; Woodhead Publ.: Oxford, 2014; pp 169–208.

(11) Iglesias, J. E.; Zuniga, F. J.; Nowacki, W. $NaAsS_2$, a Synthetic Sulfosalt Related to the NaCl Type. *Z. Kristallogr*. **1977**, *146*, 43–52.

(12) Palazzi, M. Structure Cristalline de l'Orthotrithioarsenite Trisodique, Na_3AsS_3. *Acta Crystal. B* **1976**, *32*, 3175–3177.

(13) Chaus, I. S.; Demchenko, L. E.; Sukhenko, V. D. Phase Diagram of the System Na_2S-As_2S_3. *Ukr. Khim. Zhurnal* **1974**, *40*, 473–476.

(14) Mullen, D. J. E.; Nowacki, W. Refinement of the Crystal Structures of Realgar AsS and Orpiment, As_2S_3. *Z. Kristallogr*. **1972**, *136*, 48–65.

(15) Kampf, A. R.; Downs, R. T.; Housley, R. M.; Jenkins, R. A.; Hyršl, J. Anorpiment, As_2S_3, the Triclinic Dimorph of 0rpiment. *Mineral. Mag*. **2011**, *75*, 2857–2867.

(16) Bonneau, P. R.; Jarvis, R. F. jr.; Kaner, R. B. Solid-State Metathesis as a Quick Route to Transition-Metal Mixed Dichalcogenides. *Inorg. Chem*. **1992**, *31*, 2127–2132.

(17) Kassem, M.; Khaoulani, S.; Cuisset, A.; Le Coq, D.; Masselin, P.; Bychkov, E. Mercury Thioarsenate Glasses: a Hybrid Chain/Pyramidal Network. *RSC Advances* **2014**, *4*, 49236–49246.

(18) Paraskiva, A.; Bokova, M.; Bychkov, E. Na^+ Ion Conducting Glasses in the NaCl-Ga_2S_3-GeS_2 System: a Critical Percolation Regime. *Solid State Ionics* **2017**, *299*, 2–7.

(19) Kassem, M.; Bokova, M.; Tverjanovich, A.; Fontanari, D.; Le Coq, D.; Sokolov, A.; Masselin, P.; Kohara, S.; Usuki, T.; Hannon, A. C.; Benmore, C. J.; Bychkov, E. Bent HgI_2 Molecules in the Melt and Sulfide Glasses: Implications for Nonlinear Optics, *Chem. Mater*. **2019**, *31*, 4103–4112.

(20) Hannon, A. C. Results on Disordered Materials from the General Materials Diffractometer, GEM, at ISIS. *Nucl. Instrum. Methods Phys. Res., Sect. A* **2005**, *551*, 88–107.

(21) Hannon, A. C.; Howells, W. S.; Soper, A. K. ATLAS: A Suite of Programs for the Analysis of Time-of-Flight Neutron Diffraction Data from Liquid and Amorphous Samples. *Inst. Phys. Conf. Ser*. **1990**, *107*, 193–211.

(22) Soper, A. K. GudrunN and GudrunX: Programs for Correcting Raw Neutron and X-Ray Total Scattering Data to Differential Cross Section. *GUDRUN Manual, ISIS Spallation Source* **2017**, https://www.isis.stfc.ac.uk/OtherFiles/Disordered%20Materials/Gudrun-Manual-2017-10.pdf

(23) Hutter, J.; Iannuzzi, M.; Schimann, F.; VandeVondele, J. CP2K: Atomistic Simulations of Condensed Matter Systems. *Wiley Interdisciplinary Reviews: Computational Molecular Science* **2014**, *4*, 15–25.

(24) Perdew, J. P.; Burke, K.; Ernzerhof, M. Generalized Gradient Approximation Made Simple. *Phys. Rev. Lett*. **1996**, *77*, 3865–3868.

(25) Perdew, J. P.; Ruzsinszky, A.; Csonka, G. I.; Vydrov, O. A.; Scuseria, G. E.; Constantin, L. A.; Zhou, X.; Burke, K. Restoring the Density-Gradient Expansion for Exchange in Solids and Surfaces. *Phys. Rev. Lett.* **2008**, *100*, 136406.

(26) Perdew, J. P.; Ernzerhof, M.; Burke, K. Rationale for Mixing Exact Exchange with Density Functional Approximations. *J. Chem. Phys*. **1996**, *105*, 9982–9985.

(27) Adamo, C.; Barone, V. Toward Reliable Density Functional Methods without Adjustable Parameters: The PBE0 Model. *J. Chem. Phys*. **1999**, *110*, 6158–6170.

(28) Akola, J.; Jones, R. O.; Kohara, S.; Kimura, S.; Kobayashi, K.; Takata, M.; Matsunaga, T.; Kojima, R.; Yamada, N. Experimentally Constrained Density-Functional Calculations of the Amorphous Structure of the Prototypical Phase-Change Material $Ge_2Sb_2Te_5$, *Phys. Rev. B: Condens. Matter Mater. Phys*. **2009**, *80*, 020201.

(29) Matsunaga, T.; Akola, J.; Kohara, S.; Honma, T.; Kobayashi, K.; Ikenaga, E.; Jones, R. O.; Yamada, N.; Takata, M.; Kojima, R. From local structure to nanosecond recrystallization dynamics in AgInSbTe phase-change materials, *Nature Mater*. **2011**, *10*, 129–134.

(30) Gereben, O.; Jovari, P.; Temleitner, L.; Pusztai, L. A New Version of the RMC++ Reverse Monte Carlo Programme, Aimed at Investigating the Structure of Covalent Glasses. *J. Optoelectron. Adv. Mater*. **2007**, *9*, 3021–3027.

(31) Gereben, O.; Pusztai, L. RMC_POT, a Computer Code for Reverse Monte Carlo Modeling the Structure of Disordered Systems Containing Molecules of Arbitrary Complexity. *J. Comp. Chem*. **2012**, *33*, 2285–2291.

(32) VandeVondele, J.; Hutter, J. Gaussian Basis Sets for Accurate Calculations on Molecular Systems in Gas and Condensed Phases. *J. Chem. Phys*. **2007**, *127*, 114105.

(33) Weigend, F.; Ahlrichs, R. Balanced Basis Sets of Split Valence, Triple Zeta Valence and Quadruple Zeta Valence Quality for H to Rn: Design and Assessment of Accuracy. *Phys. Chem. Chem. Phys*. **2005**, *7*, 3297–3305.

(34) Goedecker, S.; Teter, M.; Hutter, J. Separable Dual-Space Gaussian Pseudopotentials. *Phys. Rev. B: Condens. Matter Mater. Phys*. **1996**, *54*, 1703–1710.

(35) Nosé, S. A molecular dynamics method for simulations in the canonical ensemble. *Mol. Phys*. **1984**, *52*, 255–268.

(36) Hoover, W. G. Canonical dynamics: equilibrium phase-space distributions. *Phys. Rev. A: Atom., Mol., Opt. Phys*. **1985**, *31*, 1695–1697.

(37) Le Roux, S.; Jund, P. Ring Statistics Analysis of Topological Networks: New Approach and Application to Amorphous GeS_2 and SiO_2 Systems. *Comput. Mater. Sci*. **2010**, 49, 70–83.

(38) Kohara, S.; Ohno, H.; Tabaka, M.; Usuki, T.; Morita, H.; Suzuya, K.; Akola, J.; Pusztai, L. Lead Silicate Glasses: Binary Network-Former Glasses with Large Amounts of Free Volume. *Phys. Rev. B: Condens. Matter Mater. Phys*. **2010**, *82*, 134209.

(39) Heimbach, I.; Rhiem, F.; Beule, F.; Knodt, D.; Heinen, J.; Jones, R. O. pyMolDyn: Identification, Structure, and Properties of Cavities/Vacancies in Condensed Matter and Molecules. *J. Comput. Chem.* **2017**, *38*, 389–394.

(40) Lee J. H.; Owens, A. P.; Pradel, A.; Hannon, A. C.; Ribes, M.; Elliott, S. R. Structure Determination of Ag-Ge-S Glasses using Neutron Diffraction. *Phys. Rev. B: Condens. Matter Mater. Phys*. **1996**, *54*, 3895–3909.

(41) Bychkov, E.; Price, D. L. Neutron Diffraction Studies of Ag_2S–As_2S_3 Glasses in the Percolation and Modifier-Controlled domains. *Solid State Ionics* **2000**, *136–137*, 1041–1048.

(42) Itoh, K.; Fukunaga, T. Structure of Na_2S–GeS_2 Glasses Studied by using Neutron and X-ray Diffraction and Reverse Monte Carlo Modeling. *Solid State Ionics* **2009**, *180*, 351–355.

(43) Ohara, K.; Mitsui, A.; Mori, M.; Onodera, Y.; Shiotani, S.; Koyama, Y.; Orikasa, Y.; Murakami, M.; Shimoda, K.; Mori, K.; Fukunaga, T.; Arai, H.; Uchimoto, Y.; Ogumi, Z. Structural and Electronic Features of Binary Li_2S-P_2S_5 glasses. *Scientific Reports* **2016**, *6*, 21302.

(44) Bychkov, E.; Benmore, C. J.; Price, D. L. Compositional Changes of the First Sharp Diffraction Peak in Binary Selenide Glasses. *Phys. Rev. B: Condens. Matter Mater. Phys*. **2005**, *72*, 172107.

(45) Bytchkov, A.; Cuello, G. J.; Kohara, S.; Benmore, C. J.; Price, D. L.; Bychkov, E. Unraveling the Atomic Structure of Ge-Rich Sulfide Glasses. *Phys. Chem. Chem. Phys*. **2013**, *15*, 8487–8494.

(46) Benmore, C. J.; Hart, R. T.; Mei, Q.; Price, D. L.; Yarger, J.; Tulk, C. A.; Klug, D. D. Intermediate Range Chemical Ordering in Amorphous and Liquid Water, Si, and Ge. *Phys. Rev. B: Condens. Matter Mater. Phys*. **2005**, *72*, 132201.

(47) Guthrie, M.; Tulk, C. A.; Benmore, C. J.; Xu, J.; Yarger, J. L.; Klug, D. D.; Tse, J. S.; Mao, H.-K.; Hemley, R. J. Formation and Structure of a Dense Octahedral Glass. *Phys. Rev. Lett*. **2004**, *93*, 115502.

(48) Mei, Q.; Benmore, C. J.; Hart, R. T.; Bychkov, E.; Salmon, P. S.; Martin, C. D.; Michel, F. M.; Antao, S. M.; Chupas, P. J.; Lee, P. L.; Shastri, S. D.; Parise, J. B.; Leinenweber, K.; Amin, S.; Yarger, J. L. Topological Changes in Glassy $GeSe_2$ at Pressures up to 9.3 GPa Determined by High-Energy X-ray and Neutron Diffraction Measurements. *Phys. Rev. B: Condens. Matter Mater. Phys*. **2006**, *74*, 014203.

(49) E. Soignard, O. B. Tsiok, A. S. Tverjanovich, A. Bytchkov, A. Sokolov, V. V. Brazhkin, C. J. Benmore, E. Bychkov, Pressure-Driven Chemical Disorder in Glassy As_2S_3 up to 14.7 GPa, Postdensification Effects, and Applications in Materials Design. *J. Phys. Chem. B* **2020**, *124*, 430–442.

(50) Lorch, E. Neutron Diffraction by Germania, Silica and Radiation-Damaged Silica Glasses. *J. Phys. C: Solid State Phys*. **1969**, *2*, 229–237.

(51) Frumar, M.; Firth, A. P.; Owen, A. E. A Model for Photostructural Changes in the Amorphous As-S System. *J. Non-Cryst. Solids* **1983**, *59–60*, 921–924.

(52) Bychkov, E.; Miloshova, M.; Price, D. L.; Benmore, C. J.; Lorriaux, A. Short, Intermediate and Mesoscopic Range Order in Sulfur-Rich Binary Glasses. *J. Non-Cryst. Solids* **2006**, *352*, 63–70.

(53) Le Roux, S.; Bouzid, A.; Boero, M.; Massobrio, C. Structural Properties of Glassy Ge_2Se_3 from First-Principles Molecular Dynamics. *Phys. Rev. B: Condens. Matter Mater. Phys*. **2012**, *86*, 224201.

(54) Bachhuber, F.; von Appen, J.; Dronskowski, R.; Schmidt, P.; Nilges, T.; Pfitzner, A.; Weihrich, R. The Extended Stability Range of Phosphorus Allotropes. *Angew. Chem. Int. Ed*. **2014**, *53*, 11629–11633.

(55) Ohkubo, T.; Ohara, K.; Tsuchida, E. Conduction Mechanism in $70Li_2S$-$30P_2S_5$ Glass by ab initio Molecular Dynamics Simulations: Comparison with $Li_7P_3S_{11}$ Crystal. ACS Appl. Mater. Interfaces **2020**, *12*, 25736–25747.

(56) Zhou, W.; Sayers, D. E.; Paesler, M. A.; Bouchet-Fabre, B.; Ma, Q.; Raoux, D. Structure and Photoinduced Structural Changes in a-As_2S_3 Films: A Study by Differential Anomalous X-ray Scattering. *Phys. Rev. B: Condens. Matter Mater. Phys*. **1993**, *47*, 686–694.

(57) Simdyankin, S. I.; Elliott, S. R.; Hajnal, Z.; Niehaus, T. A.; Frauenheim, Th. Simulation of Physical Properties of the Chalcogenide Glass As_2S_3 using a Density-Functional-Based Tight-Binding Method. *Phys. Rev. B: Condens. Matter Mater. Phys*. **2004**, *69*, 144202.

(58) Akola, J.; Jóvári, P.; Kaban, I.; Voleská, I.; Kolář, J.; Wágner, T.; Jones, R. O. Structure, Electronic, and Vibrational Properties of Amorphous AsS_2 and $AgAsS_2$: Experimentally Constrained Density Functional Study. *Phys. Rev. B: Condens. Matter Mater. Phys*. **2014**, *89*, 064202.

(59) Akola, J.; Beuneu, B.; Jones, R. O.; Jóvári, P.; Kaban, I.; Kolář, J.; Voleská, I.; Wágner, T. Structure of Amorphous Ag/Ge/S Alloys: Experimentally Constrained Density Functional Study. *J. Phys.: Condens. Matter* **2015**, *27*, 485304.

(60) Gorochov, O. Les Composés Ag_8MX_6 (M = Si, Ge, Sn et X = S, Se, Te). *Bull. Soc. Chim. France* **1968**, *1968*, 2263–2275.

(61) Alekseev, A.; Fontanari, D.; Sokolov, A.; Bokova, M.; Kassem, M.; Bychkov, E. Ionic Conductivity and Tracer Diffusion in Glassy Chalcogenides. In *World Scientific Reference of Amorphous Materials*; Taylor, P. C., Editor-in-chief; Vol. 1; World Scientific: Singapore, 2020; pp 203–249. https://www.worldscientific.com/worldscibooks/10.1142/11697

(62) Blaineau, S.; Jund, P. Structural Properties of Various Sodium Thiogermanate Glasses through DFT-based Molecular Dynamics Simulations, *Phys. Rev. B: Condens. Matter Mater. Phys*. **2006**, *74*, 054203.

(63) Hannon, A. C. XTAL: a Program for Calculating Interatomic Distances and Coordination Numbers for Model Structures. *Rutherford-Appleton Laboratory Report RAL-93-063*, 1993. http://wwwisis2.isis.rl.ac.uk/disordered/ACH/Software/xtal.htm).

(64) Dive, A.; Zhang, Y.; Yao, Y.; Martin, S. W.; Banerjee, S. Investigations of the Structure of $Na_2S+P_2S_5$ Glassy Electrolytes and its Impact on Na^+ Ionic Conductivity through *ab initio* Molecular Dynamics. *Solid State Ionics* **2019**, *338*, 177–184.

(65) Bischoff, C.; Schuller, K.; Haynes, M.; Martin, S. W. Structural Investigations of $y$$Na_2S+(1-y)PS_{5/2}$ Glasses using Raman and Infrared Spectroscopies. *J. Non-Cryst. Solids*, **2012**, *358*, 3216–3222.

(66) Kuhn, A.; Eger, R.; Nuss, J.; Lotsch, B. V. Synthesis and Structural Characterization of the Alkali Thiophosphates $Na_2P_2S_6$, $Na_4P_2S_6$, $K_4P_2S_6$, and $Rb_4P_2S_6$. *Z. Anorg. Allg. Chem*. **2014**, *640*, 689–692.

(67) Jansen, M.; Henseler, U. Synthesis, Structure Determination, and Ionic Conductivity of Sodium Tetrathiophosphate. *J. Solid State Chem*. **1992**, *99*, 110–119.

(68) Krauskopf, T.; Culver, S. P.; Zeier, W. Local Tetragonal Structure of the Cubic Superionic Conductor Na_3PS_4. *Inorg. Chem*. **2018**, *57*, 4739–4744.

(69) Baba, T.; Kawamura, Y. Structure and Ionic Conductivity of Li_2S-P_2S_5 Glass Electrolytes Simulated with First-Principles Molecular Dynamics. *Front. Energy Res*. **2016**, *4*, 22.

For Table of Contents only

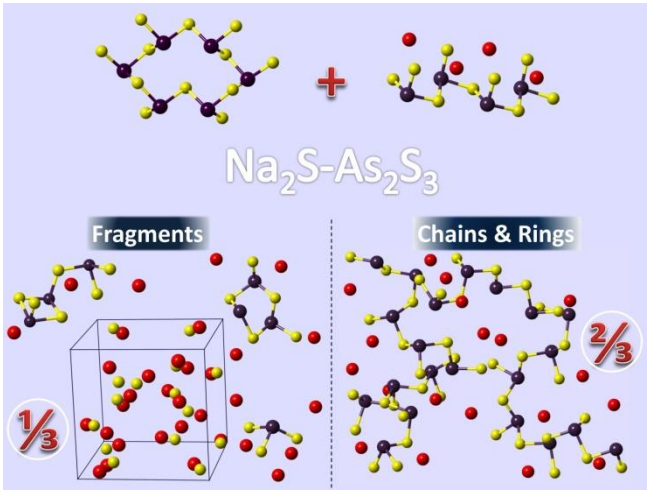

Using pulsed neutron diffraction supported by first-principles molecular dynamics, we show a structural diversity of Na_2S-As_2S_3 sodium thioarsenate glasses, basically different from structural motifs predicted by the equilibrium phase diagram.